Hindawi
Journal of Nanomaterials
Volume 2022, Article ID 6880220, 7 pages
https://doi.org/10.1155/2022/6880220

Research Article

Self-Delivering Supramolecular Nanofiber Based on Peptide-Rhein Conjugate

Jingjing Wang, Xue Rui, Zhetong Jin, Xuejiao Leng, and Zhipeng Chen

College of Pharmacy, Nanjing University of Chinese Medicine, Nanjing, Jiangsu 210023, China

Correspondence should be addressed to Zhipeng Chen; czpcpu2000@hotmail.com

Received 10 May 2022; Accepted 20 July 2022; Published 23 September 2022

Academic Editor: Mazeyar Parvinzadeh Gashti

Copyright © 2022 Jingjing Wang et al. This is an open access article distributed under the Creative Commons Attribution License, which permits unrestricted use, distribution, and reproduction in any medium, provided the original work is properly cited.

A peptide-drug conjugate (PDC) is a single molecule formed by one or more drug molecules that are conjugated with functional short peptides. Some specially designed PDC can construct self-delivering supramolecular nanomedicine and improve the therapeutic effect. The design and synthesis of novel PDCs with unique assembly behavior are important for the drug delivery system. Rhein is a natural product extracted from rhubarb and has extensive pharmacological properties. In the present work, we successfully synthesized a novel PDC (VKVK-rhein) based on rhein through solid-phase synthesis technology and conventional coupling chemical methods. The anthraquinone structure of rhein and the structure of the short peptide (VKVK, Val-Lys-Val-Lys) provided VKVK-rhein with special assembly properties. VKVK-rhein can be assembled into supramolecular nanofibers in water. The equilibrium solubility, oil-water distribution coefficient, zeta potential, and cell viability of VKVK-rhein were systematically studied. Our work lays a foundation for further biological application of rhein-based PDCs.

1. Introduction

Peptide-drug conjugates (PDCs) are therapeutic drugs that are formed by combining one or more drug molecules with short peptides [1, 2]. Various PDCs have been synthesized to improve the drug's therapeutic outcome. For example, the NGR peptide-Dau conjugates composed of asparagine-glycine-arginine (NGR) peptide and daunomycin have high antitumor activity *in vivo* [3]. The paclitaxel-Angiopep-2 conjugate, which is synthesized by paclitaxel and Angiopep-2, is effective for brain cancer treatment [4]. Peptide BP10 covalently coupling doxorubicin with disulfide bonds enhances the antitumor efficacy of triple-negative breast cancer [5]. Specially designed PDCs with assembly behavior as molecular building blocks can construct self-delivering nanomedicine [6–8], such as nanofiber, nanotube, nanobelt, and hydrogel [9–12], which have different morphologies. PDCs, as self-assembly prodrugs, have great potential in drug delivery [13, 14]. VEVE-Ket, which consists of ketoprofen and valine-glutamic acid dimeric repeat peptide, can form supramolecular filament hydrogels that can be used for the treatment of arthritic diseases [15]. A well-designed PDC directly assemble camptothecin into discrete, stable, well-defined nanostructures with a high and quantitative drug loading [16]. As can be seen from the previous examples, the design and synthesis of novel PDCs with unique assembly behavior are important for the drug delivery system.

Rhein (1,8-dihydroxy-3-carboxyanthraquinone), which mainly exists in plant rhubarb, is a lipophilic anthraquinone. Rhein has various biological activities, such as analgesic, antipyretic, anti-inflammatory, lipid-lowering, bone and joint protection, antidiabetes, and antifibrosis, and it inhibits the proliferation of various tumor cells [17–19]. Its special anthraquinone structure endows it with pharmaceutical function, but its low bioavailability limits its further application. Many drug delivery systems have been designed to improve its bioavailability. Feng et al. loaded rhein with solid lipid nanoparticles to increase oral absorption and improve the oral bioavailability of rhein [20]. A kind of rhein formulation based on poly(lactic-co-glycolic acid) nanoparticles has been developed for oral administration [21]. Nanoparticles based on β-cyclodextrin-rhein conjugate have been

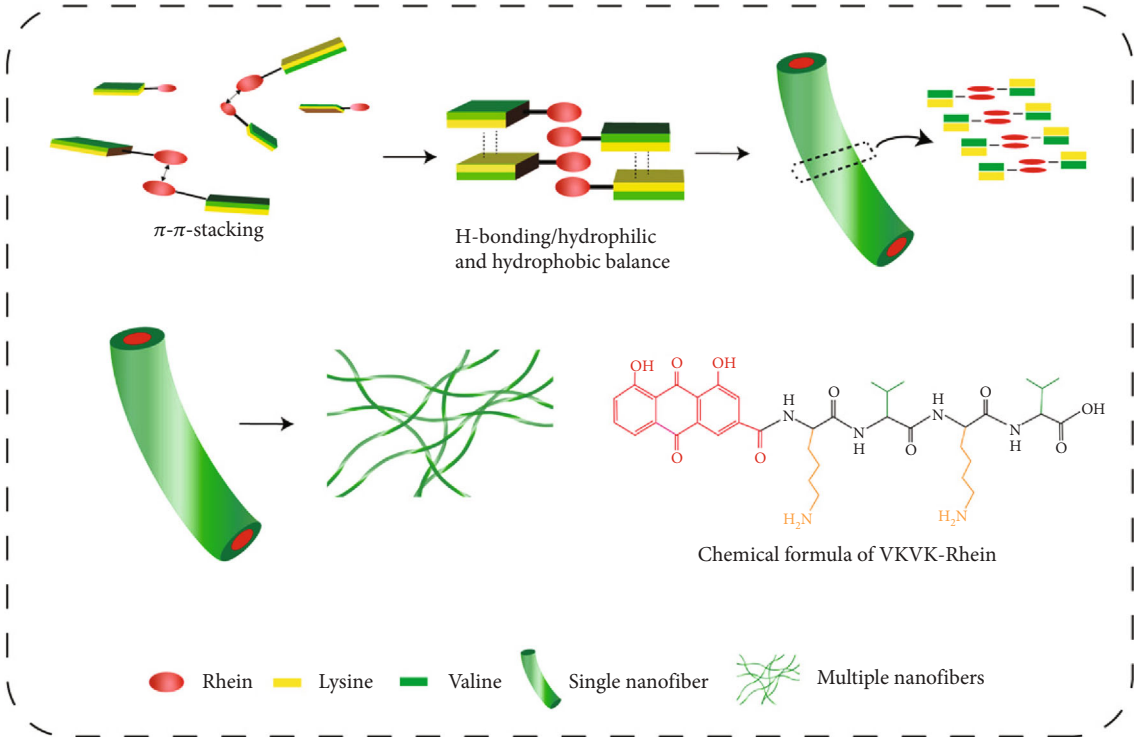

Figure 1: Scheme illustration for the assembly behavior of VKVK-rhein.

prepared to improve the bioavailability of rhein [22]. However, rhein-based PDC, as a self-delivering drug delivery system, is rarely studied.

In the present work, a novel PDC (VKVK-rhein) composed of rhein and valine-lysine dimer repeat peptide was synthesized by solid-phase synthesis and chemical coupling. VKVK-rhein can be self-assembled into self-delivering supramolecular nanofiber (Figure 1). The equilibrium solubility, oil-water distribution coefficient, chemical electromotive force, and cell viability of VKVK-rhein were systematically studied. The results provide a foundation for the further biological application of rhein-based PDCs.

2. Materials and Methods

2.1. Materials and Reagents. Fmoc-protected valine (V), Fmoc-protected lysine (K), N, N-dimethylamino-pyridine, 2-(1H-benzotriazole-1-yl)-1,1,3,3-tetramethyluronium hexafluorophosphate (HBTU), N,N-diisopropylethylamine (DIEA), dichloromethane (DCM), N,N-dimethylformamide (DMF), acetic anhydride, pyridine, piperidine, trifluoroacetic acid (TFA), triisopropylsilane (TIS), and 2-chlorotrityl chloride resin (Wang resin) were obtained from Sigma-Aldrich; HPLC-grade methanol was obtained from E. Merck (Merck, Darmstadt, Germany).

Matrix-assisted laser desorption ionization and time-of-flight mass spectrometry (MALDI-TOF MS) analysis was performed using autoflex II TOF/TOF mass spectrometer (Bruker Daltonics, Bremen, Germany). Approximately, 1 μL of VKVK-rhein solution (10 mg/mL) was spotted on a polished steel target plate and allowed to air dry. Then, 1 μL of the matrix (3,4-dimethosycinnamic acid, 10 mg/mL) was spotted on the steel target plate prior to mass analysis.

Transmission electron microscopy (TEM) was performed using a JEM-2100 microscope at a voltage of 120 kV. A drop of VKVK-rhein solution (5 mg/mL) was placed on the surface of a copper grid (400 meshes) coated with a carbon membrane, and the grids were dried at room temperature before TEM observation.

UV-vis absorption spectra (UV-VIS) were acquired in the range of 200–600 nm by using a BioMate 3S UV/visible spectrophotometer (Thermo Fisher).

2.2. Methods

2.2.1. Synthesis of VKVK-Rhein. First, KVKV-Wang resin was synthesized on a FOCUS XC (AAPPTec, Louisville, KY) by using a standard solid-phase peptide synthesis protocol. 2-Chlorotrityl chloride resin was mixed with dry DCM and bubbled with nitrogen gas (N_2) for 20 min for the resin to completely swell. Next, the first Fmoc-protected amino acid (V) was loaded onto resin via its *C*-terminal carboxylate group by bubbling the resin in a DMF solution of Fmoc-protected amino acid and DIEA for 1 h. After washing with DMF five times, the resin was bubbled with the blocking solution (80 : 5 : 15 of DMF/MeOH/DIEA) for 0.5 h to deactivate the unreacted sites. Then, the resins were reacted with 20% piperidine (in DMF) for 20 min to remove the protecting group. Afterwards, the reaction solution was washed with DMF for six times. Then, the next Fmoc-protected amino acid (K), DIEA, and HBTU were added and reacted for 0.5 h. After the reaction was completed, the solution was washed thrice with DMF and added with 20%

piperidine to remove the Fmoc-protective group on the amino acid. These two steps were repeated to elongate the peptide chain until the final tetrapeptide sequence vector was obtained. After the last amino acid was coupled and the Fmoc-protective group was removed, rhein, HBTU, and DIEA (1 : 1 : 1 mol/mol) were added to the resin and the mixture was shaken overnight. After washing with DMF five times, a negative Kaiser test was obtained showing complete reaction. The PDC was cleaved from the resin with a mixture of TFA/TIS/H_2O (95 : 2.5 : 2.5, *v*/*v*) for 2 h. The solution was concentrated and precipitated with ether. The solid was collected and dried, forming a yellow solid VKVK-rhein. The crude product was purified via high-performance liquid chromatography (HPLC).

2.2.2. Determination of Equilibrium Solubility at Different pH Values. Phosphate buffer solutions (PBS) (50 mM) with pH values of 2.0, 5.0, 5.8, 6.8, 7.4, and 8.0 were prepared in advance. Excessive amounts of rhein and VKVK-rhein were separately placed in 10 mL of PBS with different pH values and sonicated until the drug was no longer dissolved. After being shaken for 72 h at 37°C, the samples were centrifuged at 10000 rpm for 10 min. The concentration of each group was measured by HPLC. The equilibrium solubility of rhein and VKVK-rhein in each medium was calculated.

2.2.3. Oil-Water Partition Coefficient of Rhein and VKVK-Rhein at Different pH Values. N-Octanol was mixed with PBS of different pH values (2.0, 5.0, 5.8, 6.8, 7.4, and 8.0) at a volume ratio of 1 : 1. After ultrasonic blending, they were put into a thermostatic water bath shaker and shaken at 37°C for 12 h. After standing for 24 h, the two phases were separated and the lower layer was the n-octanol-saturated buffer.

An excessive amount of rhein (or VKVK-rhein) was added to n-octanol-saturated buffers with different pH values. The solution was sonicated for 10 minutes to dissolve rhein (or VKVK-rhein) and then centrifuged at 10000 rpm for 10 min. Approximately 200 μL of supernatant was detected by HPLC, and the concentration of the supernatant ($C1$) was calculated according to the standard curve of rhein (or VKVK-rhein).

Approximately 1 mL of the above supernatant and 1 mL of buffer saturated n-octanol with different pH were precisely measured and added to a 4 mL centrifuge tube. Then, the tube was placed into a thermostatic water bath shaker, which was shaken 48 h at 37°C to make the drug fully equilibrated in the two phases.

After standing for 40 min, the aqueous phase was centrifuged at 10000 rpm for 10 min. Then, 200 μL of supernatant was obtained and detected by HPLC. The peak area was recorded and the concentration ($C2$) was calculated according to the standard curve of rhein (or VKVK-rhein). The apparent oil-water distribution coefficient (log D) was calculated according to the following formula: $D = (C1 - C2)/C2$.

2.2.4. Zeta Potential. Zeta potential was measured using Zetasizer Nano ZS90 (Malvern Instruments Ltd., UK). VKVK-rhein solution with different pH values (1.0, 3.0, 5.0, 7.0, 9.0, and 11.0) was adjusted using an appropriate amount of 1 M HCl or 1 M NaOH. The surface charge of VKVK-rhein under different pH values was measured. All groups were measured in triplicate.

2.2.5. Preparation of VKVK-Rhein Supramolecular Nanofibers. Approximately 2 mg VKVK-rhein was dissolved in 10 μL of DMSO. Then, 400 μL of PBS was added to the solution to form VKVK-rhein supramolecular fibers. The morphology was observed by transmission electron microscopy.

2.2.6. Cell Viability Assay. To characterize the cytotoxicity of VKVK-rhein and rhein *in vitro*, we used colorimetric 3-(4,5-dimethyl-2-thiazolyl)-2,5-diphenyl tetrazolium bromide (MTT) assay to evaluate the proliferation of HepG2 cells. HepG2 cells in the logarithmic growth phase (1×10^5/well) were cultured in 96-well plates (100 μL/well). After incubation for 24 h, cells were individually treated with 211, 141, 106, 71, 36, 18, and 9 μM VKVK-rhein. After incubation for 24 h, 100 μL of MTT was added to each well for crystal solubilization. At 4 h after incubation, the supernatant was replaced by DMSO (150 μL) and the plate was shaken for 5 min. The optical density (OD) was measured at 490 nm by using a microplate reader.

The inhibitory rate of cell growth and the half-maximal inhibitory concentration IC_{50} values were calculated as follows: inhibition rate = [1 − (OD value of drug group/OD value of control group)] × 100%.

2.2.7. Statistical Analysis. Statistical analysis was performed using the SPSS statistical software package (version 16.0, SPSS Inc., Chicago, IL, USA). The data are presented as the mean ± SD.

3. Results and Discussion

3.1. Synthesis of VKVK-Rhein. The peptide segment on resin (KVKV-Wang Resin) was first prepared based on standard solid-phase synthesis protocols. Then, the carboxyl group on rhein was directly coupled with the amino group on KVKV-Wang resin. Finally, the drug-peptide conjugate VKVK-rhein was cleaved from the resin with TFA. Mass spectrometry and analytical HPLC were used to confirm the expected mass and purity of VKVK-rhein (Figure 2).

Based on the mass spectrum (Figure 2(a)), the excimer ion peak $[M + H]$ m/z of the sample is 739.27. The molecular fragment peak shown on the mass spectrum has been resolved, confirming that the obtained product is VKVK-rhein. Figures 2(b) and 2(c) are the HPLC spectra of rhein and VKVK-rhein. The chromatographic peak of rhein is observed at 5.6 min, and the chromatographic peak of VKVK-rhein is observed at approximately 10.5 min. The chromatogram of VKVK-rhein is considerably different from that of rhein. After analysis and calculation, the purity of the obtained product exceeded 95%. Based on the mass spectrum and liquid phase diagram, VKVK-rhein has high purity and can meet the needs of subsequent experiments.

The ultraviolet visible absorption spectroscopy results are shown in Figure 3. The covalent binding of peptide to rhein did not affect its UV absorption peak. The UV

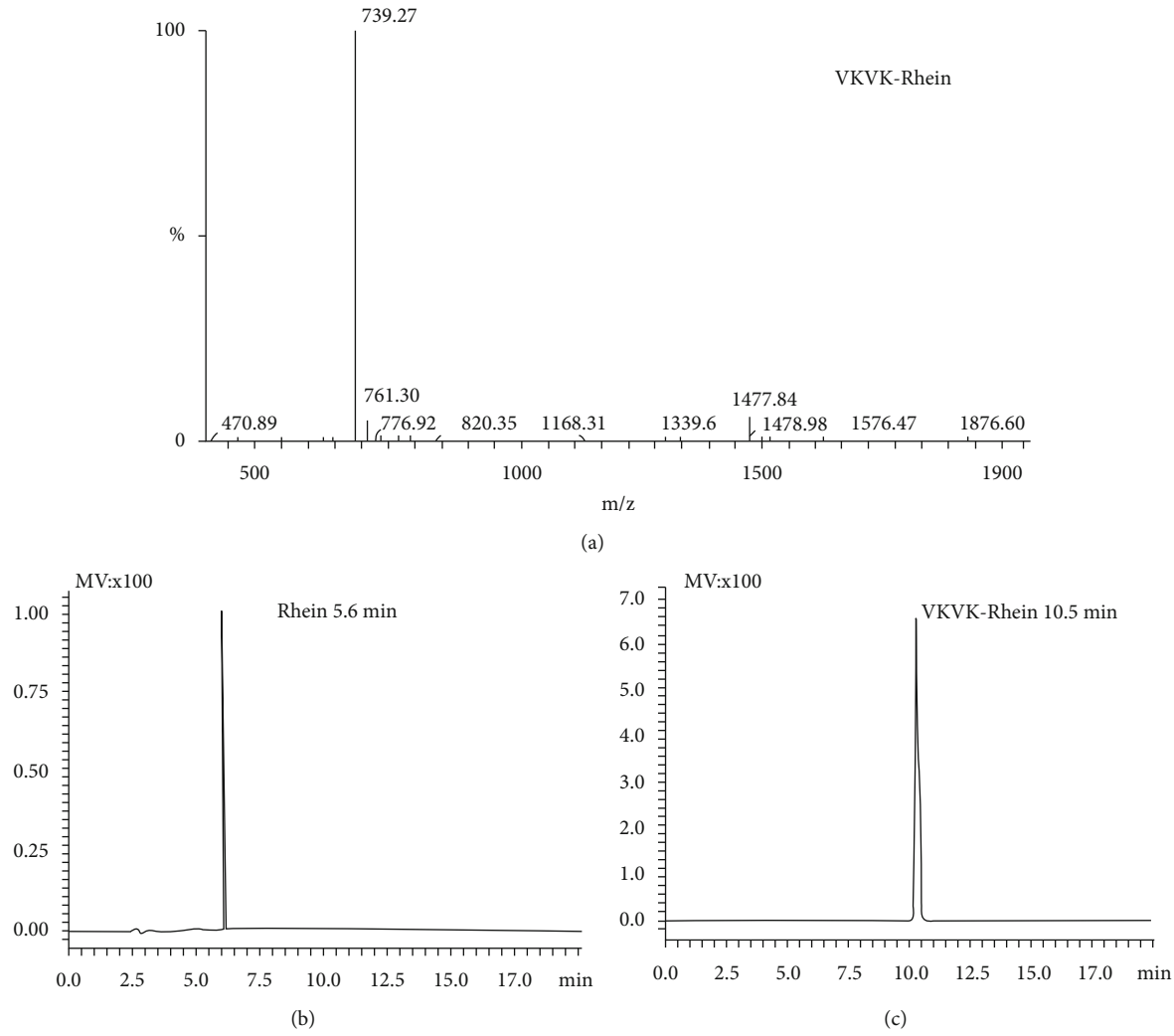

Figure 2: (a) Mass spectrum of VKVK-rhein, (b) liquid-phase diagram of rhein, and (c) VKVK-rhein.

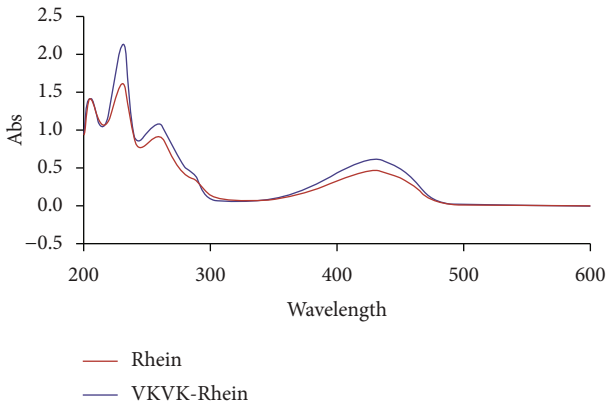

Figure 3: Ultraviolet visible absorption spectroscopy of rhein and VKVK-rhein.

absorption wavelength was 254 nm, but the intensity was reduced after the amino acid was connected, possibly because of the condensation reaction between the amino group of polypeptide and the terminal carboxyl group of rhein. The peptide sequence affected its overall electronic transition, which reduced the intensity of the absorption peak. Although the absorption intensity of rhein and VKVK-rhein differs, the wavelength of the absorption peak did not change. Therefore, the maximum absorption wavelength (254 nm) can be used as the wavelength for ultraviolet detection.

3.2. Solubility of Rhein and VKVK-Rhein at Different pH Values. The solubility of rhein and VKVK-rhein is shown in Figure 4(a). The solubility of rhein is proportional to the increase of pH, which is related to the structure of rhein. Rhein contains a carboxyl group; the increase in pH caused the carboxyl groups to dissociate gradually, thus gradually increasing the solubility. The solubility of VKVK-rhein was highest at 6.8 and then decreased, possibly because of the dissociation equilibrium between amino and carboxyl groups in the molecule. Moreover, the equilibrium solubility of VKVK-rhein in water was greater than that of rhein, indicating that the solubility of the drug was improved after the peptide was connected, and the solubility was better than that of rhein at pH 6.8.

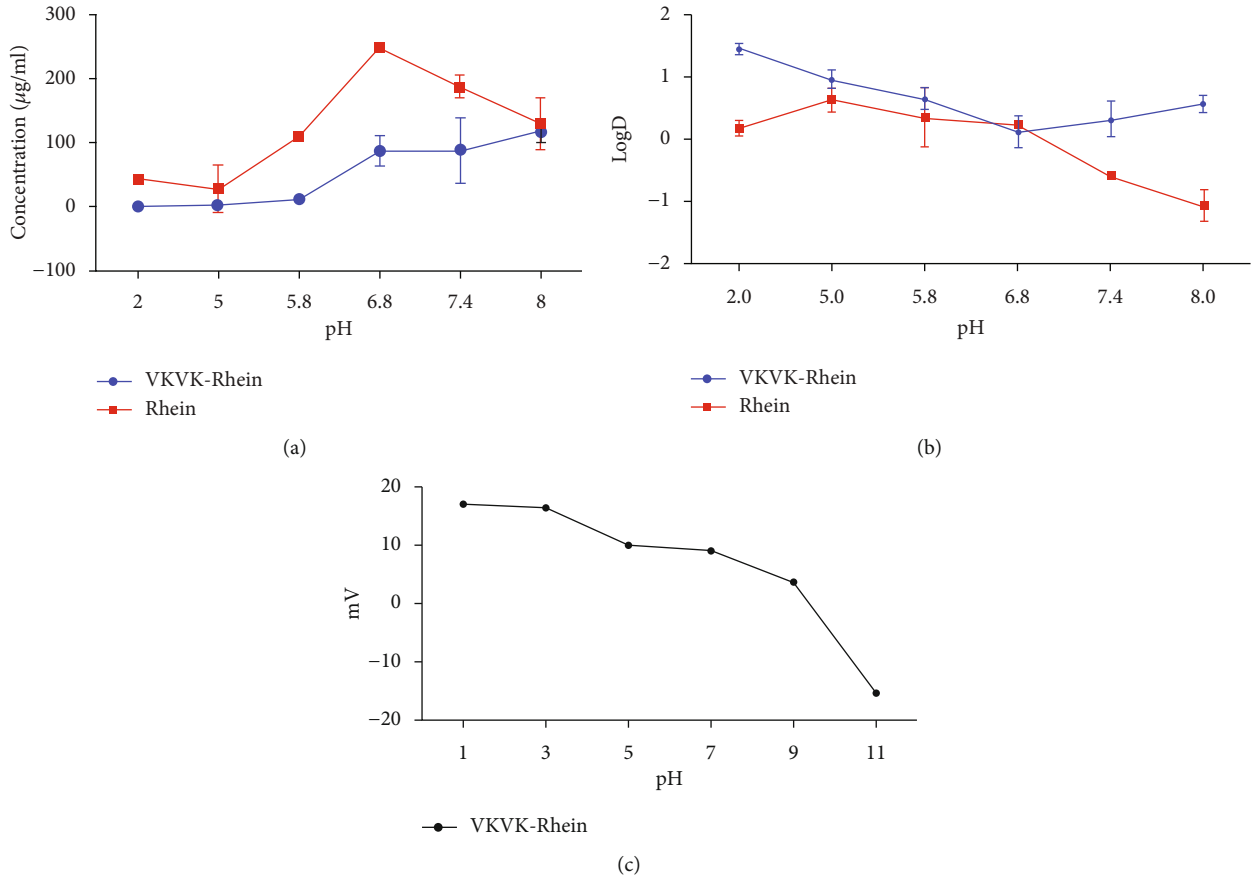

Figure 4: (a) Equilibrium solubility of rhein and VKVK-rhein at different pH values at 37°C, (b) log *D* of rhein and VKVK-rhein at different pH values at 37°C, and (c) zeta potential of VKVK-rhein at different pH values.

3.3. Oil-Water Partition Coefficients of Rhein and VKVK-Rhein at Different pH Values. The oil-water partition coefficients are shown in Figure 4(b). At pH 5–6.8, log *D* of VKVK-rhein remained stable at approximately 0.5, indicating that a stable structure may be formed during assembly. In addition, the log *D* of VKVK-rhein was stable. The log *D* of VKVK-rhein was less than that of rhein, indicating that the hydrophilicity was enhanced after the peptide had been linked to rhein and the hydrophilicity was also enhanced with the increase of pH, possibly because the carboxyl group in the drug molecule underwent dissociation under alkaline conditions. Moreover, the log *D* value at pH 3, 5, 7, and 9 was approximately 1.0.

3.4. Zeta Potential of VKVK-Rhein at Different pH Values. The results are shown in Figure 4(c). According to the structural characteristics of VKVK-rhein and the changes of zeta potential, the two amino groups in the VKVK-rhein molecule combine with H^+ in water to form positively charged NH^{3+}. With the increase of pH, the negative ions in the solution increased, resulting in the dissociation of the carboxyl group. Subsequently, the drug molecule gradually had a negative charge.

3.5. Preparation of VKVK-Rhein Supramolecular Nanofiber. The TEM pictures of VKVK-rhein supramolecular nanofiber are shown in Figure 5. The prepared nanofibers were crosslinked to each other. It had good stability and had a tendency and potential to form gels. Molecular self-assembly is caused by the interaction of noncovalent forces

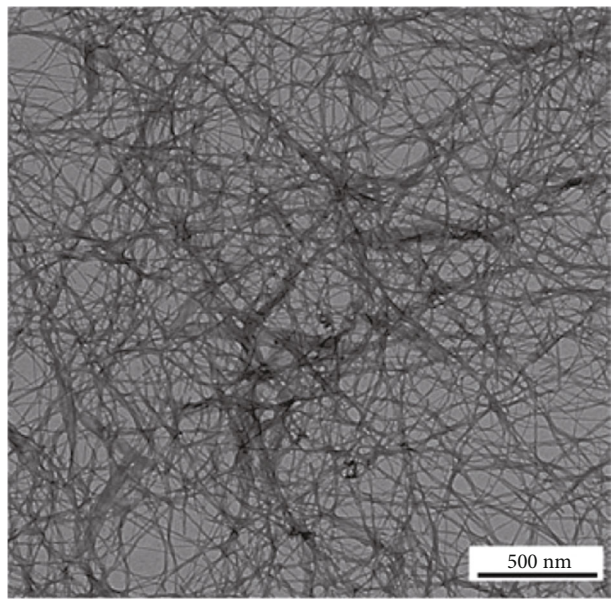

Figure 5: TEM picture of VKVK-rhein supermolecular nanofiber.

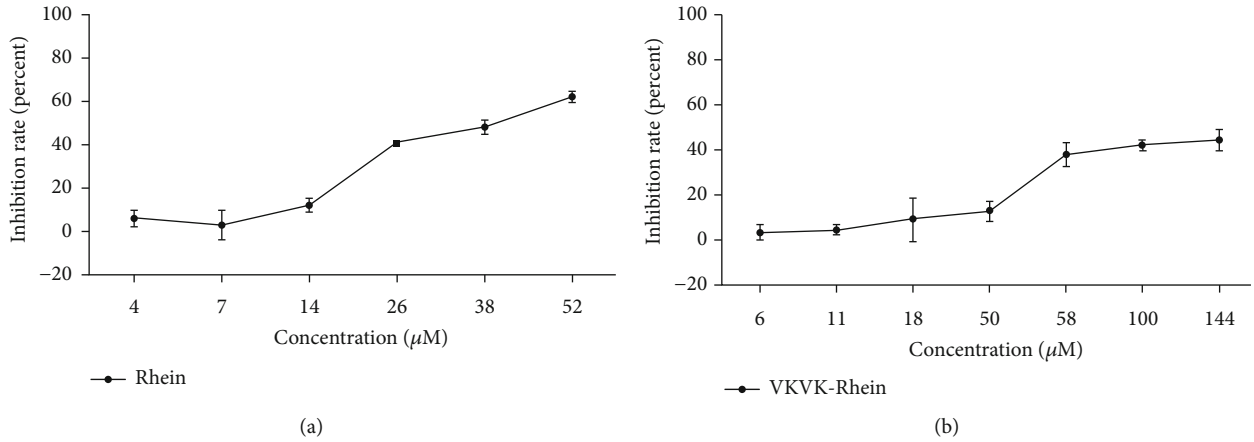

Figure 6: Concentration-inhibition curve of rhein (a) and VKVK-rhein (b) on HepG2 cells.

such as hydrogen bonding, electrostatic interaction, hydrophobic interaction, Van der Waals force, and π-π stacking. The molecular monomers aggregate and further form a supramolecular structures with special morphology and functions [23]. Molecular self-assembly has broad application prospects in biomaterials. The nanofibers assembled by VKVK-rhein could be used as a self-delivering nanocargo in drug delivery for local injection.

3.6. Cell Viability Assay. The effects of VKVK-rhein and rhein on the inhibition of HepG2 cell proliferation are shown in Figure 6. With the increase of the concentration (9–211 μM), VKVK-rhein and rhein can inhibit the proliferation of HepG2 cells in a dose-dependent manner. The IC_{50} of VKVK-rhein is 149.04 μM. The IC_{50} of rhein is 38.32 μM. It could be found that the biological activity of rhein is retained in VKVK-rhein, thus enhancing its further biological activity as self-delivering nanofibers.

4. Conclusions

A novel PDC (VKVK-rhein) containing rhein and short peptide with self-assembly behavior has been successfully synthesized. VKVK-rhein can form highly ordered nanofibers in aqueous solution as a self-delivering nanofiber with high drug loading. We systematically studied VKVK-rhein in terms of equilibrium solubility, oil-water distribution coefficient, zeta potential, and cytotoxicity assay to lay a foundation for the further biological application of rhein-based PDCs.

Data Availability

The data used to support the findings of this study are included within the article.

Conflicts of Interest

The authors declare that there are no conflicts of interest regarding the publication of this paper.

Acknowledgments

This work was supported by the National Natural Science Foundation of China (no. 32000997), Natural Science Foundation of Nanjing University of Chinese Medicine (NZY32000997), and Natural Science Foundation of the Jiangsu Higher Education Institution of China (20KJB350004).

References

[1] B. M. Cooper, J. Iegre, D. H. O'Donovan, M. O. Halvarsson, and D. R. Spring, "Peptides as a platform for targeted therapeutics for cancer: peptide-drug conjugates (PDCs)," *Chemical Society Reviews*, vol. 50, no. 3, pp. 1480–1494, 2021.

[2] B. Bumbaca, Z. Li, and D. K. Shah, "Pharmacokinetics of protein and peptide conjugates," *Drug Metabolism and Pharmacokinetics*, vol. 34, no. 1, pp. 42–54, 2019.

[3] K. N. Enyedi, S. Tóth, G. Szakács, and G. Mező, "NGR-peptide –drug conjugates with dual targeting properties," *PLoS One*, vol. 12, no. 6, article e0178632, 2017.

[4] A. Regina, M. Demeule, C. Che et al., "Antitumour activity of ANG1005, a conjugate between paclitaxel and the new brain delivery vector Angiopep-2," *British Journal of Pharmacology*, vol. 155, no. 2, pp. 185–197, 2008.

[5] C. Xiao, J. Han, J. Bai, Y. Xia, and S. Wang, "Trojan-like peptide drug conjugate design and construction for application in treatment of triple-negative breast cancer," *Journal of Biomedical Nanotechnology*, vol. 17, no. 8, pp. 1554–1563, 2021.

[6] C. Gao, P. Bhattarai, M. Chen et al., "Amphiphilic drug conjugates as nanomedicines for combined cancer therapy," *Bioconjugate Chemistry*, vol. 29, no. 12, pp. 3967–3981, 2018.

[7] J. Wang, Y. Qian, L. Xu et al., "Hyaluronic acid-shelled, peptide drug conjugate-cored nanomedicine for the treatment of hepatocellular carcinoma," *Materials Science & Engineering. C, Materials for Biological Applications*, vol. 117, article 111261, 2020.

[8] Q. Fan, Y. Ji, J. Wang et al., "Self-assembly behaviours of peptide-drug conjugates: influence of multiple factors on aggregate morphology and potential self-assembly mechanism," *Royal Society Open Science*, vol. 5, no. 4, article 172040, 2018.

[9] F. Wang, H. Su, D. Xu et al., "Tumour sensitization via the extended intratumoural release of a STING agonist and camptothecin from a self-assembled hydrogel," *Nature Biomedical Engineering*, vol. 4, no. 11, pp. 1090–1101, 2020.

[10] C. Qian, J. Wang, Y. Qian et al., "Tumor-cell-surface adherable peptide-drug conjugate prodrug nanoparticles inhibit tumor metastasis and augment treatment efficacy," *Nano Letters*, vol. 20, no. 6, pp. 4153–4161, 2020.

[11] Y. Sun, Y. Liang, W. Dai et al., "Peptide-drug conjugate-based nanocombination actualizes breast cancer treatment by maytansinoid and photothermia with the assistance of fluorescent and photoacoustic images," *Nano Letters*, vol. 19, no. 5, pp. 3229–3237, 2019.

[12] T. Hao, Y. Fu, Y. Yang et al., "Tumor vasculature-targeting PEGylated peptide-drug conjugate prodrug nanoparticles improve chemotherapy and prevent tumor metastasis," *European Journal of Medicinal Chemistry*, vol. 219, article 113430, 2021.

[13] Y. Wang, A. G. Cheetham, G. Angacian, H. Su, L. Xie, and H. Cui, "Peptide-drug conjugates as effective prodrug strategies for targeted delivery," *Advanced Drug Delivery Reviews*, vol. 110-111, pp. 112–126, 2017.

[14] K. Kalishwaralal, G. Luboshits, and M. A. Firer, "Synthesis of gold nanoparticle: peptide-drug conjugates for targeted drug delivery," *Methods in Molecular Biology*, vol. 2059, pp. 145–154, 2020.

[15] Z. Chen, L. Xing, Q. Fan et al., "Drug-bearing supramolecular filament hydrogels as anti-inflammatory agents," *Theranostics*, vol. 7, no. 7, pp. 2003–2014, 2017.

[16] A. G. Cheetham, P. Zhang, Y. A. Lin, L. L. Lock, and H. Cui, "Supramolecular nanostructures formed by anticancer drug assembly," *Journal of the American Chemical Society*, vol. 135, no. 8, pp. 2907–2910, 2013.

[17] Z. Xian, J. Tian, L. Wang et al., "Effects of rhein on bile acid homeostasis in rats," *BioMed Research International*, vol. 2020, Article ID 8827955, 13 pages, 2020.

[18] D. M. Barbosa, P. Fahlbusch, D. Herzfeld de Wiza et al., "Rhein, a novel histone deacetylase (HDAC) inhibitor with antifibrotic potency in human myocardial fibrosis," *Scientific Reports*, vol. 10, no. 1, pp. 1–13, 2020.

[19] B. Ren, W. Guo, Y. Tang et al., "Rhein inhibits the migration of ovarian cancer cells through down-regulation of matrix metalloproteinases," *Biological & Pharmaceutical Bulletin*, vol. 42, no. 4, pp. 568–572, 2019.

[20] H. Feng, Y. Zhu, Z. Fu, and D. Li, "Preparation, characterization, and in vivo study of rhein solid lipid nanoparticles for oral delivery," *Chemical Biology & Drug Design*, vol. 90, no. 5, pp. 867–872, 2017.

[21] Z. Yuan and X. Gu, "Preparation, characterization, and in vivo study of rhein-loaded poly(lactic-co-glycolic acid) nanoparticles for oral delivery," *Drug Design, Development and Therapy*, vol. 9, pp. 2301–2309, 2015.

[22] J. Wang, Y. Qian, C. Qian et al., "A novel β-cyclodextrin-rhein conjugate for improving the water solubility and bioavailability of rhein," *Carbohydrate Research*, vol. 490, article 107958, 2020.

[23] Y. Li, X. Zheng, Z. Cao, W. Xu, J. Zhang, and M. Gong, "Self-assembled peptide (CADY-1) improved the clinical application of doxorubicin," *International Journal of Pharmaceutics*, vol. 434, no. 1-2, pp. 209–214, 2012.